Pedestal Studies at ASDEX Upgrade

E. Wolfrum, R. Fischer, B. Langer, T. Pütterich, G.D. Conway, D.P. Coster, R. Dux, J.C. Fuchs, M. Gemisic Adamov, N. Hicks, L.D. Horton, C. Konz, B. Kurzan, K. Lackner, C.F. Maggi, P.J. McCarthy, M. Reich, J. Schweinzer, W. Suttrop, C. Tröster and ASDEX Upgrade Team

Max Planck Institut für Plasmaphysik, EURATOM Association, D-85748 Garching, Germany

E-mail: e.wolfrum@ipp.mpg.de

Abstract
The ASDEX Upgrade suite of edge pedestal diagnostics has been significantly improved. A new edge ion temperature and toroidal velocity diagnostic as well as a novel diagnostic for radial electric fields (E_r) have been added. The application of integrated data analysis in a probabilistic framework contributes substantially to the quality of E_r and electron density profiles. The equilibrium reconstruction, taking into account scrape off layer (SOL) tile currents, renders equilibria on a 1 ms time base, which are used for mapping edge profile data synchronized to edge localised modes (ELMs). An example is shown, where the width of the pedestal pressure increases with NBI heating power, which can be assigned to ion and electron temperature profiles. The analysis of profiles over an ELM cycle shows that conclusions regarding the convective or conductive nature of an ELM can only be drawn with an accurate knowledge of the plasma position.

1. Introduction

The increase in confinement occurring at the transition from L-mode to H-mode is widely assumed to be a consequence of reduced turbulent transport at the plasma edge, coinciding with the creation of an edge transport barrier (ETB) also called pedestal. The pedestal top temperature affects the global confinement if stiff temperature profiles create a link between the pedestal and the core regions as usually observed in H-mode plasmas /1/. The top of the pedestal has also been associated with the energy loss during an ELM event /2/ and is found to be the origin of filamentary structures transporting plasma into and across the scrape off layer /3/. Properties of the ETB and its breakdown during ELMs are studied at ASDEX Upgrade in order to explore the transport and related turbulent structures, to set boundary conditions for theoretical calculations and to provide significant experimental data for ELMs in various scenarios.
For these investigations the accurate determination of profiles of plasma parameters such as electron temperature (T_e), electron density (n_e), ion temperature (T_i), toroidal velocity (v_{tor}), and radial electric field (E_r) are essential. In the first part of this paper recent improvements and developments of diagnostics measuring the above mentioned parameters at ASDEX Upgrade are reported and the alignment of the various diagnostics to each other is described. In the second part we present selected results regarding the edge transport barrier, i.e. (i) the change of ETB width with heating power and (ii) n_e and T_e profile development during an ELM cycle.

2. Profile measurements

At ASDEX Upgrade a large effort was put into a series of improvements to existing pedestal diagnostics as well as the implementation of two new diagnostic systems for the measurement of edge T_i and v_{tor} profiles from charge exchange spectroscopy and for the determination of radial electric fields from passive He II emission. Probabilistic data analysis was used in

several applications: (i) to improve n_e evaluation from Lithium beam emission profiles, (ii) to evaluate E_r from passive He II emission, and (iii) for Integrated Data Analysis (IDA). In the framework of Bayesian probability theory the posterior probability distribution function (pdf) is proportional to the likelihood pdf, describing the misfit between the modelled and measured data, and the prior pdfs, describing all additional information /4/. The method of IDA combines data from heterogeneous and complementary diagnostics within a full probabilistic framework to obtain most reliable results. Redundancy of different diagnostics is exploited to provide information for the removal of data inconsistencies.
In the following only recent improvements to diagnostics or new ones are described, while other edge pedestal diagnostics such as Thomson scattering /5/ or Doppler reflectometry /6/ are still important elements of the ASDEX Upgrade edge diagnostic suite.

2.1. n_e profiles

The probabilistic data analysis method is applied to analyze the spatially resolved beam emission profiles of the lithium beam diagnostic /7/. The method yields density profiles with a spatial resolution of 5 mm and a temporal resolution of 50 μs. Profiles in the edge region can be fully explored up to a pedestal top density of 8 10^{19} m^{-3}. Additionally, IDA was applied to the reconstruction of n_e profiles from the lithium beam (LIB) and the DCN interferometry data /8/ to obtain full profiles, i.e. across the whole plasma cross section. Using LIB data only allows inferring the profile up to the pedestal, where the pedestal densities become quite uncertain. Combining LIB and DCN interferometry data gives full density profiles where the pedestal density is robustly estimated. As next step Thomson scattering data will be included in the IDA analysis of an integrated n_e profile. Figure 1 shows n_e profiles resolving an ELM with pedestal top uncertainties largely reduced due to IDA of LIB and DCN diagnostics.

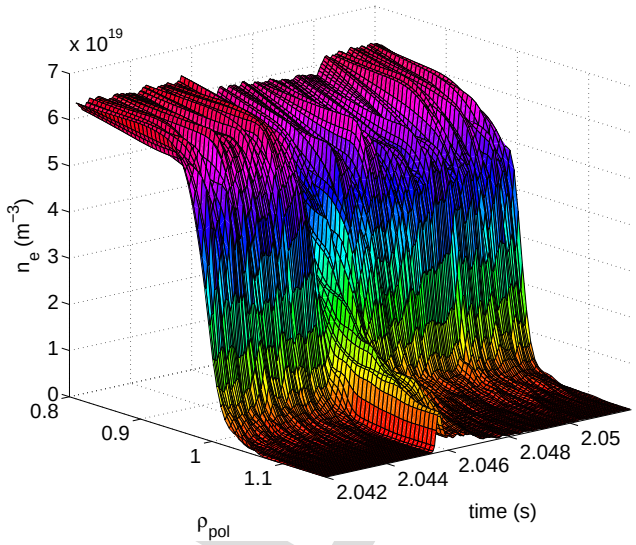

Figure 1: Electron density profiles (AUG #22561) resolve ELMs with 50 μs temporal and 5 mm spatial resolution. Pedestal top uncertainties are largely reduced due to integrated data analysis of Li-beam and DCN interferometer diagnostic.

2.2. T_e profiles

A 60 channel super-heterodyne radiometer for the measurement of second harmonic X-mode ECE is employed along a horizontal line of sight near the tokamak mid plane. The system yields radial T_e profiles with spatial resolution ~ 10 mm, and has recently been upgraded with a new data acquisition system with sampling rate 1 MHz /9/. The original data acquisition with sampling rate 31.25 kHz has been retained in parallel for validation. The fast data acquisition allows measurements of plasma phenomena on the MHD timescale, such as neoclassical tearing modes or ELMs, as well as studying filamentary structures which can also be observed in the inter-ELM phase (see figure 5).

2.3. T_i and v_{tor} profiles

A new diagnostic based on charge exchange recombination spectroscopy on one of the heating beams has been installed with the aim to resolve the plasma edge in H-mode discharges /10/. Great care had to be taken in order to obtain the best possible spatial resolution, minimizing the spatial extent of the emitting volumes for each line of sight (LOS). In toroidal viewing geometry a separate mirror for each LOS is used. Each of the 8 LOS is equipped with three optical fibres with 400 μm diameter. The light of the fibres is dispersed by a high throughput spectrometer (f/4, f=280 mm) equipped with a frame transfer CCD with electron multiplying readout. 15 channels (a subset of the 24 fibres) are recorded with a repetition time of 1.9 ms. Spectra of C VI or B V are fitted with two Gaussians to take into account passive components, the width of the active component yielding T_i and the line shift the toroidal velocity of the impurity ions. For profile shapes which exhibit a large gradient in intensity the radial resolution of these measurements is strongly enhanced compensating the detrimental effect of plasma curvature within the observed beam width. Moreover, best radial resolution is achieved by the routinely applied radial sweep of the plasma by ~2 cm, thereby moving the edge region through the view of the LOS.

2.4. E_r profiles

A new method to determine the radial electric field at the plasma edge has been developed which is based on passive spectroscopy of the He II line at 468.57 nm. The optical head of the Lithium beam diagnostic is used probing the plasma nearly poloidally. The observed spectra are modelled taking into account the relevant atomic processes leading to the occupation of the $He^+(n=4)$ state as well as the forces which act on the emitting particles, such as the force due to the radial electric field and the diamagnetic force due to the pressure gradient. The corresponding drift velocities v_{ExB} and v_{dia} as well as v_{tor} are used to calculate the spectrally resolved He II profile at 100 positions along each LOS which are subsequently integrated to yield a line integrated He II spectrum. The line integrated spectrally and temporally resolved data are modelled and the radial electric field is calculated by means of an IDA approach applying Bayesian probability theory /11/. Input from other sources includes the equilibrium, n_e and T_e profiles, the photon emission coefficients, and v_{tor}, the latter being constructed from the outermost data points of the core CXRS system ($0.9 < \rho_{pol} < 0.95$) and decreasing to 0 at $\rho_{pol} = 1.1$ with a similar shape as the T_i profile. Estimates of the profiles of E_r, T_{He+} and n_{He+} and the corresponding errors are obtained from the maximum and width of the posterior pdf, respectively.

2.5. Profile alignment

In order to obtain consistent profiles across the whole ETB and to reduce the uncertainty in position as given by the various diagnostics, the profiles are combined. As the ETB is only ~10-20 mm wide, it is important to achieve a relative positioning of the various diagnostics to better than 3 mm. In H-modes, where steep gradients allow an accurate relative positioning, the profiles of the various diagnostics are selected temporally relative to the occurrence of ELMs (ELM synchronized).

The various diagnostics are distributed over different toroidal and poloidal locations, and the respective profiles are mapped to the midplane. As the Thomson scattering diagnostic provides n_e and T_e measurements from the same scattering volumes, it is highly important for the alignment of n_e and T_e measurements of other diagnostics, such as ECE and Lithium beam. In the context of this paper we always refer to the edge setting of the ASDEX Upgrade Thomson scattering diagnostic (YAG) /12/. Especially for modelling transport in the transition region of closed flux surfaces to the scrape off layer (SOL) the determination of the separatrix position is essential. The electron temperature at the separatrix is linked to the

power flux across the separatrix due to the strong dependence of the parallel conductivity on T_e. The separatrix temperature can be estimated with a simple two-point model /13/ with an accuracy of ~3 mm in discharges with steep profiles, and depending on the heating power of the discharge T_e^{sep} lies between 70 and 140 eV for H-modes. This is used to determine the separatrix position more accurately than available from equilibrium reconstruction. For relative alignment of all diagnostics we start with setting T_e (YAG) to fulfil the condition for T_e^{sep}. The ECE data are then aligned to the YAG data in the upper ETB region, where second harmonic X-mode emission is optically thick. n_e profiles from the Lithium beam are then aligned to the measurements of Thomson scattering, the latter building the connection between T_e and n_e profiles. Relative positioning of edge CXRS data with an accuracy of 2-3 mm is done such that the steep T_i gradient region coincides with that of the T_e measurements.

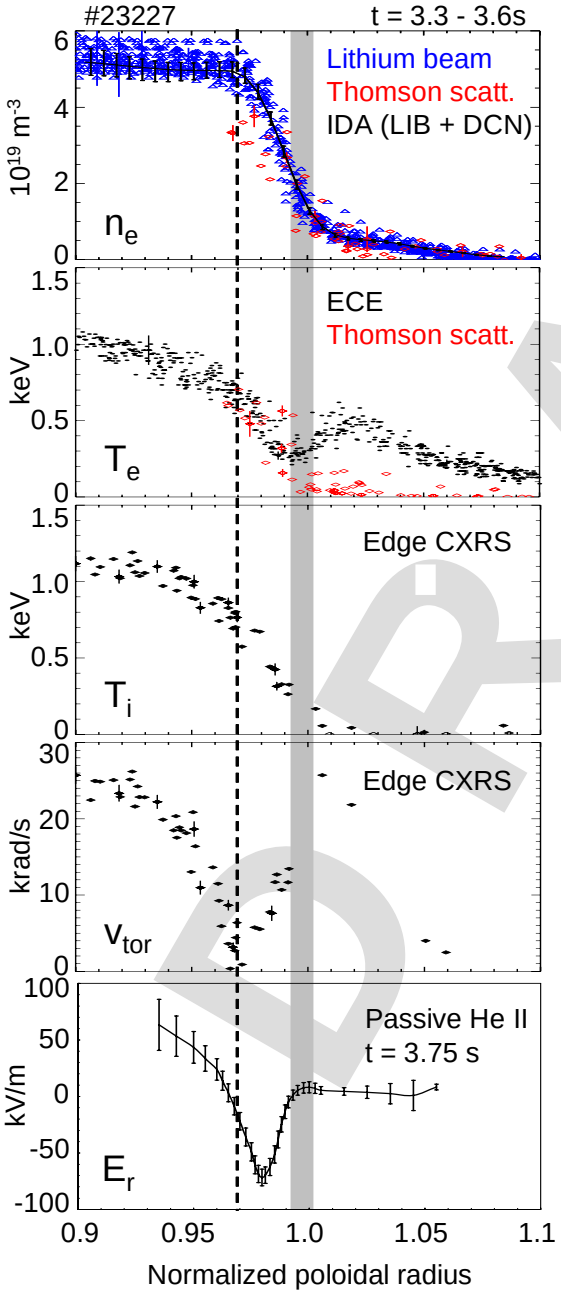

Figure 2: ELM synchronized (3.5 - 0.5 ms before ELM) profiles of n_e, T_e, T_i, v_{tor} and E_r taken during a radial shift of the plasma (# 23227, 3.3-3.6s).

v_{tor} profiles stem from the same diagnostic as T_i, so that both profiles have fixed positions relative to each other. E_r profiles are reconstructed with a set of n_e and T_e profiles as input and consequently have a fixed radial position relative to these.

Figure 2 shows an example of well aligned ELM-synchronized profiles for n_e (Thomson scattering and Li-beam), T_e (Thomson scattering and ECE: Note the strong shine-through from relativistically downshifted emission from the plasma core, which is not reabsorbed in the SOL because of its low optical depth.), T_i and v_{tor} during a radial shift of the plasma by 2.5 cm in discharge #23227. Only data which lie in the time window of -3.5 to -0.5 ms before an ELM are chosen. Additionally, one n_e profile derived by IDA (LIB + DCN) at t = 3.408 s is plotted together with its uncertainties. The inter-ELM E_r profile is derived from data at t = 3.7 s averaged over 100 ms, which is a phase in the discharge without radial shift but still the same plasma conditions. Details of this discharge will be given in the next section.

The grey bar denotes the uncertainty in the separatrix position. In the ETB zone just inside the separatrix the data exhibit excellent radial resolution and low uncertainties. In the near SOL the data are more fragmented for various reasons: edge Thomson data show a large scatter in the data due to the filamentary structure of the plasma, while the Lithium beam data cannot resolve fast fluctuations. The edge CXRS diagnostic does not deliver information in the SOL, as the impurity ion

density (here B^{5+}) drops rapidly. E_r profiles can only be derived in the region of He II emission, i.e. for $T_e > \sim 20$ eV. With all profiles aligned we can make several observations: 1.) The ETB width is narrower for n_e than for T_e and T_i. 2.) T_e and T_i barrier widths are similar. 3.) T_i at the separatrix is larger than T_e by about a factor of 2. 4.) The position of the dip in v_{tor} corresponds to the position of the 'knee' at the pedestal top in the n_e profile as indicated by the dotted line, i.e. we find evidence for strong inversed shear of toroidal rotation in the region with steep gradients in the n_e, T_e and T_i profiles. 5.) The position of the dip in E_r corresponds to the maximum of $\nabla p_i/n$. If $\nabla p_i/n$ were the determining term for E_r in the radial force balance, a minimal E_r of -80 kV/m at $\rho_{pol} \sim 0.985$ would have to be expected for this discharge. Note that for the determination of E_r a continuously decreasing v_{tor} profile is taken, so that inclusion of the increase in v_{tor} in the ETB region is estimated to give a correction of ~ +10 kV/m. Future work will include measured v_{tor} profiles as shown in this figure.

3. Example for ETB width development with increased NBI heating power

An inter-machine comparison has shown /14/ that the variation of the pedestal parameters is continuous, as the input power is increased. The pedestal top pressure is found to increase moderately with net input power as $p_{PED} \sim P_{NET}^{0.31}$. As an example for the profile development with increased NBI heating power discharge #23227 was chosen. The main plasma parameters are I_p=1 MA, B_t=-2.5T, and line averaged n_e between 6 and 7.5 10^{19} m^{-3}. Significant time traces are shown in figure 3: while electron cyclotron heating was kept constant at a level of 1.2 MW, NBI heating was ramped up in three steps from 5 MW to 7.5 MW to 10 MW. At the end of the 5 MW phase, gas fuelling was set to zero, leading to improved confinement in the high power phases /15/ as well as to a reduction of the ELM frequency from ~120 Hz (t<2.5s) to 80-90 Hz (t >2.5s). Three radial shifts of the plasma were carried out to improve the spatial resolution of the edge diagnostics. In figure 4 n_e, T_e and T_i profiles for the three phases with different heating powers are shown, which are derived from fits to ELM synchronized data collected during the radial shifts of the plasma: in black for 5 MW from 2.1-2.35s, in blue for 7.5 MW NBI from 3.0-3.6s, in red for 10 MW from 4.9-5.2s. Only data which are collected -3.5 ms to -0.5 ms before an ELM were considered, the alignment procedure described in section 2.5 was applied and a modified hyperbolic tangent curve was fitted to the data /16/.

While the pedestal widths hardly change from 5 MW to 7.5 MW heating power, which coincides with an increase in pedestal top pressure at reduced n_e, at 10 MW the pedestal width is clearly increased due to wider T_e and T_i profiles. Typical for beam fuelling only, the n_e profiles hardly change from 7.5 MW to 10 MW NBI heating power /17/, whereas the larger densities across the whole ETB at 5 MW are due to the substantial gas puff during this phase of the discharge.

Also shown in figure 4 are the ratios of gradient lengths L_x ($L_x = |1/x\ dx/dR|^{-1}$) of density to temperature, i.e. $\eta_{e,i} = L_{ne}/L_{Ti,e}$. Previously, η_e was shown to be around 2 /18/ in the ETB region for 'clean' type-I ELMs, which is also found in the case of 7.5 MW NBI heating power with $\eta_e = 1.8$. For the other two cases, i.e. 5 MW with substantial gas fuelling and 10 MW without gas fuelling, η_e is found to be around 1.2 at $0.985 < \rho_{pol} < 0.995$. For all three heating levels η_i is lower than η_e, but they assume more and more similar values as the heating power is increased. The values for η have also been determined with density and temperature profiles shifted against each other within our uncertainty of 3 mm. The values for η_e and η_i stay between 0.8 and 2 in the steep gradient region of the ETB, with η_i always lower than η_e. This is consistent with the assumption that the electron drift wave is the dominant mode at the plasma edge /19/. As the threshold for ion temperature gradient (ITG) modes lies around η_i =1 /20/, only a small shear flow is sufficient to suppress such modes. With radial electric fields as shown in figure 2, ITG modes will be completely suppressed in the ETB region.

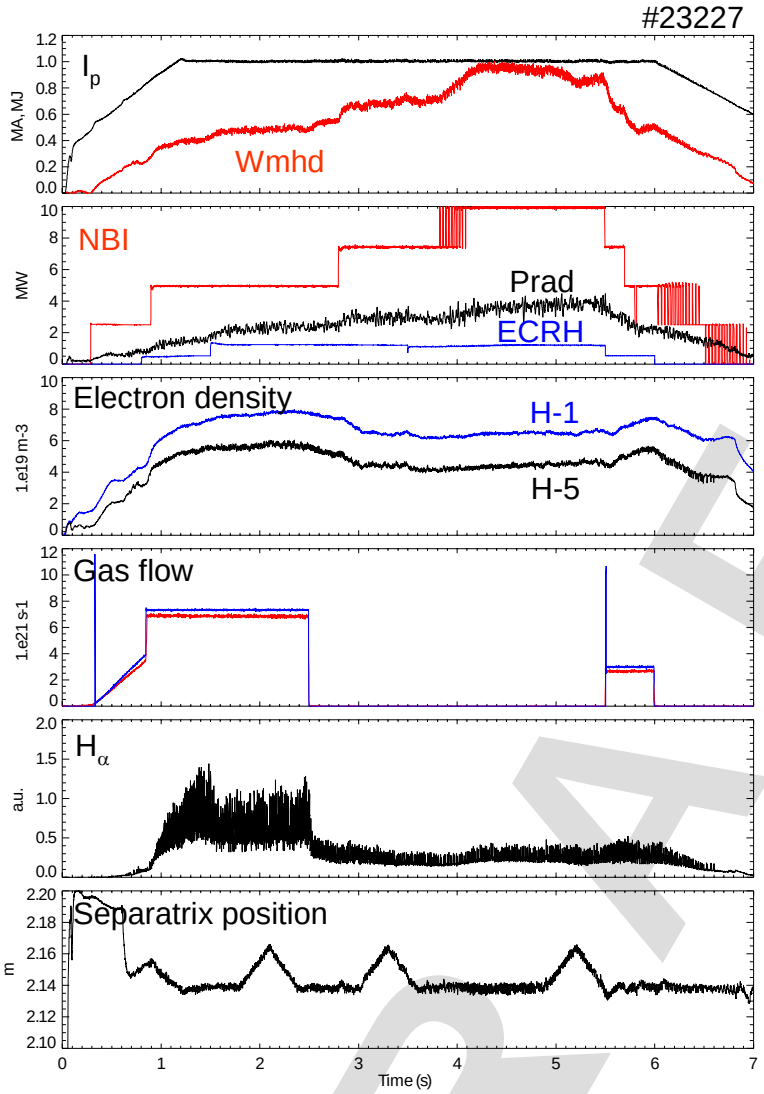

Figure 3: Time traces of discharge #23227 with (from top to bottom): plasma current (I_p), plasma energy (W_{mhd}), neutral beam heating power (NBI), electron cyclotron heating power (ECRH), radiated power (Prad), line averaged density from DCN measurements (H-1, central channel, and H-5, edge channel), gas flow, H_α radiation in the divertor, and separatrix position.

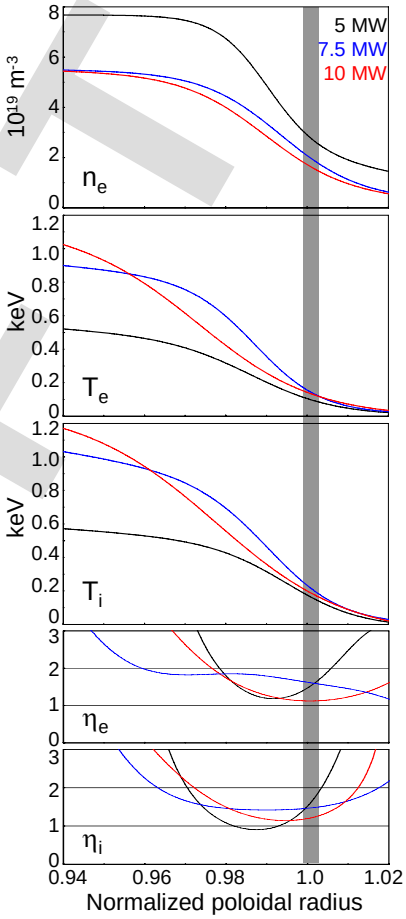

Figure 4: Pre-ELM profiles of n_e, T_e, T_i, η_i and η_e (dotted lines) for the three phases with different NBI heating power: 5 MW in black, 7.5 MW in blue and 10 MW in red.

4. ELM resolved measurements

Edge profile analysis across an ELM cycle has been carried out at ASDEX Upgrade analyzing data from profile reflectometry /21/ and Thomson scattering /22/. Electron density profiles from IDA exhibit largely reduced pedestal top uncertainties with profiles integrated over 50 microseconds. Together with the fast ECE diagnostic (1 MHz) and equilibrium reconstructions on a millisecond time base, a new quality of datasets is available for investigations of fast events such as ELMs. In the following the temporal evolution of profiles during one ELM is shown, with a pedestal top collisionality (calculated for ρ_{pol}=0.95) $\nu^* \sim 0.2$ and $q_{95} = 4.7$. From previous investigations /23/ as well as from the time traces of T_e alone, as will be shown, we would expect that this ELM would carry a considerable amount

of conductive losses. Detailed analysis, taking into account the complex changes in equilibrium and the concurrent reduction in plasma size, reveals a different picture.
In the top two frames of figure 5 time traces of n_e (LIB) and T_e (ECE) of three channels situated in the ETB region are shown. The chosen time span includes two type-I ELMs. The channels of n_e radially match the ones of T_e. The n_e time traces show that with the ELM crash the n_e ETB gradient virtually disappears, slowly recovering afterwards within 5-6 ms. The middle T_e time trace (channel 47) is one of the new 1 MHz ECE channels, whereas the other two are from the old 32 kHz system for comparison. The 1 MHz channel is noisier due to the higher bandwidth of plasma black-body fluctuations. Also shown is one magnetic signature, the positions of inner and outer separatrix, as well as the poloidal currents from shunt measurements in the outer divertor target plates, Ipolsola. An equilibrium reconstruction with a 1 ms temporal resolution taking into account the target plate currents /24/ was used to derive n_e profiles (IDA with LIB and DCN) and T_e profiles from ECE. For three timepoints during the ELM cycle the profiles are plotted in figure 6. t_1 is in the middle of the ELM cycle, t_2 2 ms before the ELM crash and t_3 2.5 ms after the ELM crash.

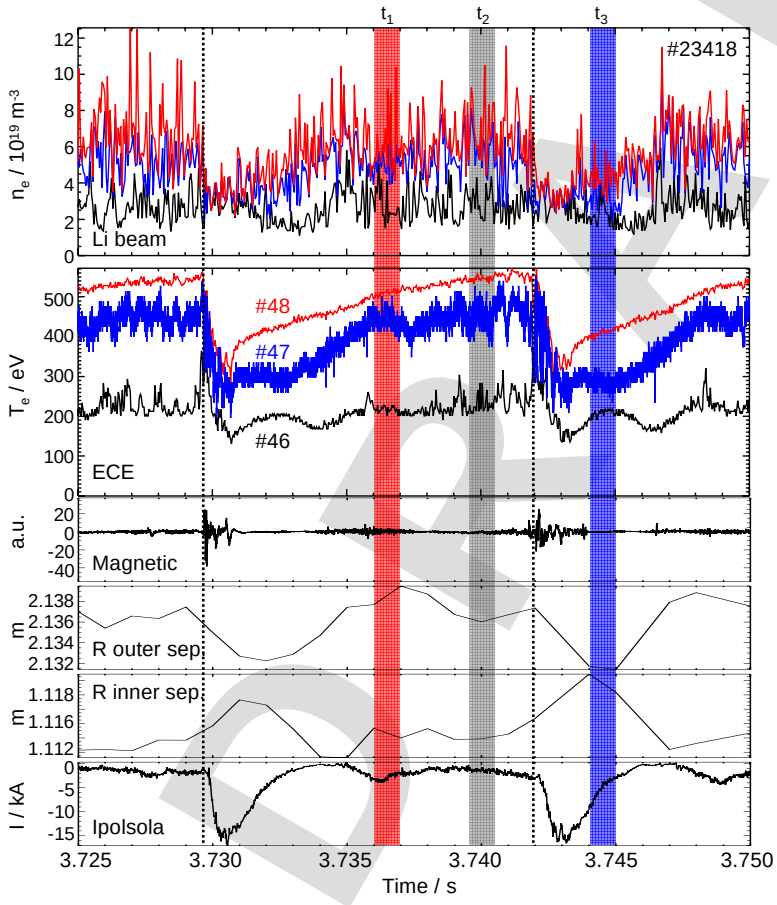

Figure 5: Time traces spanning two ELM events of discharge #23418: three n_e channels (LIB), three T_e channels (ECE), one Mirnov coil (magnetic), outer separatrix position, inner separatrix position, and shunt measurements of poloidal currents in the outer divertor (Ipolsola).

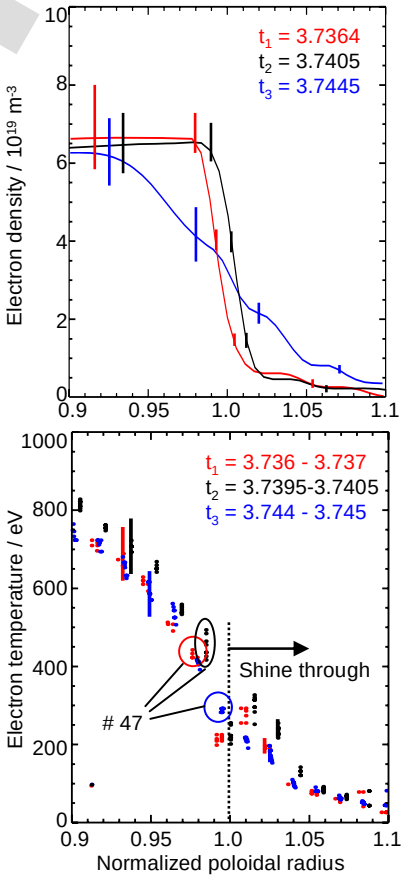

Figure 6: Mapped profiles of n_e (top) and T_e (bottom) for the three times as indicated in fig. 5: red: t_1 (in between ELMs), black: t_2 (before ELM), blue: t_3 (after ELM).

From the T_e time traces alone, not taking into account any plasma movements during the ELM cycle, one would conclude that the ELM causes a drop in T_e at the pedestal of about 200 eV. However, the traces of the outer and inner separatrix show that the plasma size changes, the ELM causing a significant reduction in plasma size.
If the ELM breakdown is at least partly driven by a peeling instability, it will also lead to a flattening of the current density gradient over the separatrix, and hence to currents flowing in the SOL. These toroidal currents will be nearly force-free (the pressure gradients in the SOL are small) and therefore will have to be accompanied by poloidal halo-currents, closing through the divertor structures. These halo-currents, in a similar fashion as in the case of vertical displacement events, will lead to a vertical net force on the plasma, and hence a change in its equilibrium configuration. The halo-currents are measured (Fig. 5, signal Ipolsola) and had already previously been used as additional input to full equilibrium reconstructions /24/. There, the observation of a small positive current spike at the ELM was reported and explained, in analogy to the case of a major disruption, as inductive reaction to the outward current rearrangement.
Using such accurate equilibrium reconstruction (note that the equilibrium used here does not contain restrictions due to the kinetic profiles), the profiles mapped to the midplane and plotted versus normalized poloidal radius do not show a significant change in T_e at the pedestal top. Comparing the n_e profiles at t_2 and t_3 reveals a small shift of the separatrix position, which is within the uncertainty of the equilibrium reconstruction. Correcting for this uncertainty such that the n_e profiles match each other, even the T_e profiles at t_2 (2 ms before the ELM) move closer to the ones at t_1 and t_3.The data show that electron temperatures adjust very quickly to the new separatrix position, with not only the same gradient but also the absolute values already recovered when the density gradient is still flat.
Such data will allow distinguishing between models for ELMs, such as convective or conductive regimes as suggested in /23/. The consistency of energy loss from the midplane determined from such data with measurements in the divertor will be investigated.

References

/1/ J. Stober et al., Plasma Phys. Controlled Fusion 42 (2000) A211
/2/ A.W. Leonard et al., Plasma Phys. Controlled Fusion 48 (2006) A149
/3/ A. Kirk et al., Phys.Rev.Lett. 96 (2006) 185001
/4/ R. Fischer et al., Rev. Sci. Instrum. 75 (2004) 4237
/5/ H. Murmann et al., Rev. Sci. Instr. 63 (1992) 4941
/6/ G. Conway et al., Proc. 8th Intl. Reflectometer Workshop for Fusion Diagnostics, IRW8, St. Petersburg, Russia, (2007), p30
/7/ R. Fischer et al., Plasma Phys. Controlled Fusion 50 (2008) 085009
/8/ O. Gehre, Int. J. of Infrared and Millimeter Waves 5 (1984) 369
/9/ N.K. Hicks et al., to be published in Proc. 15th Joint Workshop ECE and ECRH (2008)
/10/ T. Pütterich et al., 35th EPS Conf. on Plasma Physics (Hersonissos, Greece, 2008) P2.083
/11/ E. Wolfrum et al., 35th EPS Conf. on Plasma Physics (Hersonissos, Greece, 2008) O2.002
/12/ B. Kurzan et al., Plasma Phys. Controlled Fusion 46 (2004) 299
/13/ J. Neuhauser et al, Plasma Phys. Controlled Fusion 44 (2002) 855
A. Kallenbach et al., J.Nucl.Materials 337-339 (2005) 381
/14/ C.F. Maggi et al., Nucl.Fusion 47 (2007) 535
/15/ A.C.C. Sips et al, accepted for publication in Plasma Phys. Controlled Fusion (2008)
/16/ R.J. Groebner et al., Nucl. Fusion 41 (2001) 1789
/17/ C.F. Maggi et al., 35th EPS Conf. on Plasma Physics (Hersonissos, Greece, 2008) P2.024
/18/ J. Neuhauser et al., Plasma Phys. Controlled Fusion 44 (2002) 855
/19/ G. Conway et al., Nucl. Fusion 46 (2006) S799
/20/ B. Scott, New J. Phys. 4 (2002) 52
/21/ I. Nunes et al., Nucl. Fusion 44 (2004) 883
/22/ B. Kurzan et al, Plasma Phys. Controlled Fusion 49 (2007) 825
/23/ A. Loarte et al., Physics of Plasmas 11 (2004) 2668
/24/ P. McCarthy et al., 30th EPS Conf. on Plasma Physics (St.Petersburg, 2003) P1.64